Geosci. Model Dev. Discuss., 8, 4781–4821, 2015
www.geosci-model-dev-discuss.net/8/4781/2015/
doi:10.5194/gmdd-8-4781-2015

Geoscientific Model Development Discussions
Open Access

Modelling spatial and temporal vegetation variability with the Climate Constrained Vegetation Index: evidence of CO_2 fertilisation and of water stress in continental interiors

S. O. Los

Department of Geography, Swansea University, Swansea SA2 8PP UK

Received: 20 May 2015 – Accepted: 26 May 2015 – Published: 22 June 2015

Correspondence to: S. O. Los (s.o.los@swansea.ac.uk)

Published by Copernicus Publications on behalf of the European Geosciences Union.

Abstract

A model was developed to simulate spatial, seasonal and interannual variations in vegetation in response to temperature, precipitation and atmospheric CO_2 concentrations; the model addresses shortcomings in current implementations. The model uses the minimum of 12 temperature and precipitation constraint functions to simulate NDVI. Functions vary based on the Köppen–Trewartha climate classification to take adaptations of vegetation to climate into account. The simulated NDVI, referred to as the climate constrained vegetation index (CCVI), captured the spatial variability ($0.82 < r < 0.87$), seasonal variability (median $r = 0.83$) and interannual variability (median global $r = 0.24$) in NDVI. The CCVI simulated the effects of adverse climate on vegetation during the 1984 drought in the Sahel and during dust bowls of the 1930s and 1950s in the Great Plains in North America. A global CO_2 fertilisation effect was found in NDVI data, similar in magnitude to that of earlier estimates (8 % for the 20th century). This effect increased linearly with simple ratio, a transformation of the NDVI. Three CCVI scenarios, based on climate simulations using the representative concentration pathway RCP4.5, showed a greater sensitivity of vegetation towards precipitation in Northern Hemisphere mid latitudes than is currently implemented in climate models. This higher sensitivity is of importance to assess the impact of climate variability on vegetation, in particular on agricultural productivity.

1 Introduction

Spatial, seasonal and interannual variations in vegetation in response to climate affect vegetation photosynthesis and the global carbon cycle, hydrological cycle and energy budget. Feedbacks between the land surface (soil moisture and vegetation) on the one hand and the atmosphere (water, carbon and energy fluxes) on the other can enhance or mitigate the effects of climate variability or can improve forecasting of precipitation (Beljaars et al., 1996; Los et al., 2006; Taylor and Ellis, 2006). The realistic simulation of spatial and temporal variability in vegetation is therefore important, but the ability to do so is limited in current land-surface parameterisations and ecosystem models. For example, Randerson et al. (2009), using the community land model (CLM) version 3 (Dickinson et al., 2006) found a difference of up to 3 months between modelled and measured timing of maximum leaf area. Richardson et al. (2012) tested 14 commonly used land-surface parameterizations on 10 sites across North America and found large discrepancies between seasonal and interannual variations in observed and modelled leaf area index (LAI). Los et al. (2013) found that leaf seasonality simulated with the Joint UK Land Environment Simulator (JULES) (Best et al., 2011; Clark et al., 2011) south of the Sahara did not match satellite observations. Anav et al. (2013) calculated spatial correlations between Northern Hemisphere (> 30° N) LAI from 11 earth system models and satellite derived LAI; these correlations varied between $0.21 < r < 0.66$; i.e. at best 44 % of the spatial variance in observed leaf area index was explained. There is therefore a clear need for improved simulations of spatial and temporal variability of vegetation in models.

Temporal and spatial variability in vegetation parameters (leaf area index or associated parameters) is generally modelled as a function of temperature, e.g. growing degree days, and of soil moisture or drought stress (Metherall et al., 1993; Haxeltine and Prentice, 1996; Sitch et al., 2003; Knorr et al., 2010). Other, related approaches exist, e.g. Lieth's Miami model estimates annual potential net primary productivity (NPP) as the minimum of two constraints; one dependent on mean annual temperature and the other on annual precipitation (Lieth, 1975). The Miami model captures spatial and temporal variations in NPP well (Los, 2015) although some interannual variability in NPP is lost (Malmström et al., 1997). The Miami model uses an annual time step, although adaptations exist to obtain smaller, e.g. monthly time steps Esser et al. (1994). The Reconstructed Vegetation Index (RVI) (Los et al., 2006; Los, 2013) simulates monthly NDVI values from monthly precipitation and temperature using an empirical model that is optimised for each location across the global land surface. The RVI reproduces spatial, seasonal and interannual variability well (Los, 2013). A disadvantage of the RVI is that equations are optimised for current climatic conditions. It is therefore likely that the RVI is less suitable for simulations where climate deviates from current conditions. Examples are glacial periods or climate regimes that may occur if atmospheric CO_2 concentrations and global temperatures continue to rise.

A related issue is that a range of land-surface parameterizations and ecosystem models use current representations of land cover to derive biophysical parameters (Sellers et al., 1996; Potter et al., 1993; Knorr et al., 2010). These representations cannot be used without modification for scenarios under different climate regimes.

In the present study, a model was developed that uses atmospheric CO_2 concentrations, precipitation and temperature as inputs to simulate spatial, seasonal and interannual variability in leaf area and associated parameters globally (Sect. 2). The model can be applied to a range of climate scenarios, including those from the recent geological past as well as climate change scenarios with increased atmospheric CO_2 concentrations and elevated temperatures. Equations describing the constraints of precipitation and temperature on NDVI were derived for each of the six main Köppen–Trewartha climate zones A–F (Trewartha and Sale, 1968) (Sect. 3). These equations used different lags – up to 3 months and annual for precipitation and up to two months for temperature. Analogous to the Miami model Lieth (1975), the minimum of the precipitation and temperature constraints was selected to represent the NDVI. The resulting estimate of NDVI was referred to as the climate constrained vegetation index (CCVI; Sect. 3). An adjustment was made for non-linearities between the simulated CCVI and observed (1982–1999) NDVI (Sect. 3). In Sect. 4 the CCVI fields were tested against AVHRR data (1982–1999, i.e. compared to the same data used to derive the CCVI model), against MODIS data (2001–2010, which were not used to derive the CCVI model), phenology data at local sites – predominantly from the second half of the 20th century – and the global, monthly reconstructed vegetation index (1901–2006; Los et al., 2006; Los, 2013). When tested on well-known extreme events – the North American dust bowl during the 1930s and 1950s and the 1984 drought in the Sahel, south of the Sahara – the CCVI simulates a large decrease in NDVI (Sect. 4). A CO_2 fertilisation effect on NDVI was estimated from residuals between model and observations (Sect. 4). Application of the CCVI to climate change scenarios indicated a greater sensitivity of vegetation to changes in precipitation in the interiors of North America and Eurasia than found in other land-surface parameterisations (Sect. 4).

2 Data

The fused Advanced Very High Resolution Radiometer (AVHRR; 1982–1999) and Moderate Resolution Imaging Spectroradiometer (MODIS; 2001–2010) Fourier Adjusted, Solar and sensor zenith angle corrected, Interpolated and Reconstructed (FASIR) Normalised Difference Vegetation Index (NDVI) data for 1982–2010 were used (Los, 2013). This data set is corrected for sensor degradation of the AVHRRs, bidirectional effects, atmospheric scattering and absorption; outliers are removed and missing data filled in (Los, 1993, 1998b; Los et al., 2005, 2000; Sellers et al., 1996; James and Kalluri, 1994; Vermote et al., 2001)

The Climate Research Unit (CRU) time series (TS) monthly, global air surface temperature and precipitation data version 3.21 at $0.5^{\circ} \times 0.5^{\circ}$ were used (Harris et al., 2014). The data set extends from 1901 to 2013.

Mauna Loa monthly atmospheric CO_2 concentrations for 1958–2010 were obtained from NOAA (Keeling et al., 1976; Thoning et al., 1989) and were extended back to 1901 with the annual CO_2 records from the Law Dome DE08, DE08-2, and DSS ice cores (Etheridge et al., 2001).

Three gridded monthly precipitation, temperature and leaf area index products based on representative concentration pathway RCP4.5 climate simulations over 2006–2100 were obtained for the Max Planck Institute Earth System Model (Giorgetta et al., 2013), the Met Office Hadgem-CC model (Collins et al., 2011) and the NSF/DOE NCAR (National Center for Atmospheric Research Community Earth System Model coupled to the BioGeochemical Cycles model (CESM1-BGC) (Kay et al., 2014). The scenarios form part of the coupled model intercomparison project phase 5 (CMIP 5) (Taylor et al.,

GMDD
8, 4781–4821, 2015

2012). These fields, together with the 4.5 mid-year greenhouse gas concentrations for 2006–2100 (Meinshausen et al., 2011) were used to simulate global, monthly CCVI (Sect. 4).

3 Method

The six major Köppen–Trewartha climate regions (Sect. 3.1) were used to allow for climate dependent variations in precipitation and temperature constraints on NDVI (Sect. 3.2). The CCVI was calculated at monthly time step, but higher temporal resolution can be obtained by using moving monthly windows over a shorter, e.g. daily, time step.

3.1 Köppen–Trewartha classification

The Köppen–Trewartha (KT) classification was used to stratify the globe into similar climatic regions because it closely resembles the distribution of global vegetation cover and can be derived using only precipitation and temperature data. Implementation of this classification scheme in ecosystem models and land-surface parameterisations is therefore straightforward. The KT classification adapts to different climate regimes and can be updated on an annual basis in transient model simulations.

In Table 1 the rules are set out to obtain the 6 major KT classes (A–F). Class BS serves, in the present study, as an intermediate between class A and B and contains 50 % of both. Two modifications were made to the KT classification. The first was that cold deserts were grouped into class D, E or F because analysis of temperature constraints on NDVI showed that at low temperatures NDVI values were higher in cold deserts than in warm deserts (Sect. 3.2). The second modification was that transitions between classes C and D, D and E and E and F were considered to be continuous.

Continuous transitions between classes C, D, E and F were modelled using the total number of months during a 30 year period with mean temperature above 10 °C, $N_{T>10}$,

GMDD
8, 4781–4821, 2015

Title Page
Abstract Introduction
Conclusions References
Tables Figures
◂ ▸
Back Close
Full Screen / Esc
Printer-friendly Version
Interactive Discussion

rather than the total number of months from a 30 year average climatology commonly used in the KT classification scheme. The total number of months above 10 °C was divided by the length of the time period (30 years); $N_{T>10}$ becomes thus a fraction. The continuous transitions were calculated as follows: 25 and 75 % values were calculated from the $N_{T>10}$ frequency distributions for the classes C, D, E and F. Transitions between C and D were changed proportionally from the 25 % value of C (lower number of warm days in class C) to the 75 % value of D (higher number of warm days in class D). Transitions between D and E and E and F were calculated similarly. The continuous transitions ensured smooth changes in CCVI values across KT classes (Sect. 3.2).

Table 2 provides a comparison of the SIB classification developed by EROS Data Center (Loveland et al., 2001) and the major KT classes derived in the present study (using the discrete KT classification). The agreement is for the most part logical and misclassifications occur only in a few instances, e.g. for evergreen broad leaf trees in KT classes D–F) and for trees with ground cover, ground cover and shrubs with ground cover – in KT class B. The occurrence of agriculture in KT class F is unlikely as well.

3.2 Climate constraints on NDVI

The approach to simulate NDVI was based on that of the Miami model (Lieth, 1975). The Miami model calculates annual potential net primary productivity (NPP) as the minimum of two constraints; one based on temperature and the other on precipitation (Fig. 1). The spatial and temporal variations in Miami NPP correlate well with those in satellite observations (Los, 2015), although not all variability is captured and NPP derived from satellite data appears more realistic (Malmström et al., 1997). One limitation using just 2 functions to predict NDVI for the globe is that adaptations of vegetation to different climate regimes cannot be taken into account (Sect. 3.2).

A leaf seasonality model, implemented in a land-surface model or ecosystem model, can only use antecedent conditions as input. Therefore, the model was set up to calculate end-of-month NDVI values (rather than average monthly values that represent the middle of the month) from average monthly temperature and total monthly precipita-

GMDD
8, 4781–4821, 2015

tion. End-of-month NDVI values were calculated as the average of month t and month $t+1$. For precipitation seven constraints on NDVI were calculated and for temperature five. The constraints were calculated for individual months at different lags as well as for combinations of multiple months and in one case (precipitation) the total annual value was used (Table 3). The number of combinations of months included was based on a sensitivity analysis on a sample data set; inclusion of the last case (average total precipitation over past 3 months) resulted in only a small improvement. For each of the cases included, the independent variable (precipitation or temperature) was divided into 64 intervals and the 95 percentiles of NDVI distributions were calculated for each interval. Separate cases were considered for ascending NDVI ($\mathrm{NDVI}_t > \mathrm{NDVI}_{t+1}$) and descending NDVI ($\mathrm{NDVI}_t < \mathrm{NDVI}_{t+1}$), since hysteresis is frequently observed in the response of NDVI to climate. Figure 2 shows examples of precipitation and temperature constraints for ascending NDVI and several KT classes. Note that for colder KT classes, the temperatures around the freezing point show higher NDVI values; e.g. the class E NDVI value around the freezing point is about 0.4 whereas the class C NDVI value is around 0.2.

3.3 Segmented regression

Equations describing the 95th NDVI percentile as a function of climate were estimated using segmented regression (Muggeo, 2003, 2008). Segmented regression has several advantages: inflation of deviations from the mean model is smaller for linear segments than for quadratic or higher order polynomials. In addition, segmented regression is flexible and can be used without a priori knowledge of a relationship between two variables (e.g. logarithmic, exponential or quadratic). Finally, compared to the use of polynomial functions, segmented regression is less likely to give pathological predictions for values outside the range for which the functions were derived. There is a disadvantage to segmented regression in that it has a subjective element – the number of segments is chosen by the user – and solutions obtained for the same number of segments are not unique because breakpoints between segments are calculated

GMDD
8, 4781–4821, 2015

using a random number generator. Solutions are often close, however. For the present application, it was thought that the advantages, i.e. greater flexibility and smaller errors, outweighed the disadvantages, i.e. introducing a degree of arbitrariness.

For each solution varying numbers of segments were tried using different starting values. Solutions were visually inspected, and were only selected when functions were gradually changing, had preferably one maximum and had ascending NDVI at the low range of the independent variable.

A potential pitfall in deriving the NDVI vs. temperature relationships is that, by their very nature, the KT classes are defined for only a limited range of temperatures and, as a result, fitted functions may not reflect the true relationship at the high and low temperature boundaries. Therefore 95 NDVI percentiles for temperatures of adjacent classes were used, but with a much lower weighting, to guide the curve fitting at the temperature boundaries. This affected function estimation at the lower and/or upper end of the temperature range for KT classes C, D, E and F.

CCVI was calculated as the minimum of 12 climate functions representing the ascending NDVI; if $\mathrm{CCVI}_t < \mathrm{CCVI}_{t-1}$ the minimum of the 12 climate constraints for descending NDVI was used. The observations showed that the minimum monthly NDVI over the year was in about 95 % of the cases higher than 60 % of the average of 12 preceding NDVI values. The minimum of the CCVI was therefore set at 60 % of the 12 month average. The version of the CCVI thus calculated is referred to as the CCVI control.

3.4 CCVI adjustment

The CCVI control for 1982–1999 was compared with monthly FASIR NDVI data of the same period. The comparison was carried out separately for each KT class (A–F; 6 cases), both types of constraint (precipitation or temperature limited; 2 cases) and ascending and descending CCVI (2 cases). Thus for a total of $6 \times 2 \times 2 = 24$ cases, estimated CCVI (independent variable) was compared with observed FASIR NDVI (dependent variable). The independent variable was divided in 64 intervals and the average for each interval calculated. Adjustment functions were calculated using segmented linear regression (Fig. 3) and the CCVI was adjusted accordingly. This version of the CCVI is referred to as the CCVI adjusted V_{Cad}.

The mean annual CCVI and the mean CCVI for January and July for the period of 1982–1999 are shown in Fig. 4a, c, and d and are compared with the FASIR NDVI data for the same periods (Fig. 4b, d and f). Deviations between the two products are in general small ($E_{RMS} = 0.11$ for January; $E_{RMS} = 0.12$ for July and $E_{RMS} = 0.09$ for the mean annual average; Fig. 4). Relatively large biases occur in high northern latitudes during winter when no satellite observations are available and FASIR data are interpolated. A bias up to 0.1 NDVI occurs during the summer in the northern boreal forests where FASIR data are higher. However, it is likely that, after the BRDF correction, a residual positive bias with an absolute range between 0.03 and 0.05 NDVI remains in the FASIR NDVI data in high latitudes (Los et al., 2005) and this explains 30 to 50 % of the bias in the CCVI.

3.5 CO_2 fertilisation

Los (2013) found that about 40 % of the increase in NDVI over 1982–1999 could be attributed to increased atmospheric CO_2 concentrations and 40 % to trends in climate, predominantly temperature. The magnitude of the CO_2 fertilisation effect on NDVI was estimated from residuals between modelled RVI and observed NDVI. A similar approach can be used to estimate CO_2 fertilisation effect by comparing the CCVI and NDVI. However, the match between CCVI and NDVI is not as close as between RVI and NDVI and the estimation of the CO_2 fertilisation effect was therefore adapted as follows. First, the anomalies of the CCVI (departures from monthly means) were subtracted from the FASIR NDVI to eliminate climate related variability in FASIR NDVI. Then, the monthly adjusted FASIR NDVI and mean monthly observed FASIR NDVI were converted to simple ratio using the transformation $SR = (NDVI + 1)/(1 - NDVI)$. For each $0.5^\circ \times 0.5^\circ$ cell and month, the ratio between the adjusted FASIR SR and mean monthly observed FASIR SR for 1982–1999 was calculated. The ratios were

GMDD
8, 4781–4821, 2015

aggregated by KT class and changes in the ratio were expressed as functions of atmospheric CO_2 concentrations using robust linear regression (Rousseeuw and Leroy, 1987):

$$\frac{\mathrm{SR}\{V_i - \mathrm{anom}(V_{i,\mathrm{Cad}})\}}{\mathrm{SR}\{V_{i,\mathrm{seas}}\}} = \beta_0 + \beta_1[\mathrm{CO_2}] \quad (1)$$

with V_i all observed NDVI values for KT class A–E (excluding transition zones; data for F were not included because the number of observations was small); $\mathrm{anom}(V_{i,\mathrm{Cad}})$ the anomalies of the adjusted CCVI (departure of monthly mean), and $V_{i,\mathrm{seas}}$ the seasonal (monthly mean) NDVI and SR the simple ratio. Coefficients β_0 and β_1 show a close linear relationship when plotted against mean SR for each KT class (Fig. 5):

$$\beta_0 = 1.28551 - 0.25776 \times \mathrm{SR}\{V_{i,j,t}\} \quad (2)$$
$$\beta_1 = -7.950 \times 10^{-4} + 7.119 \times 10^{-4} \times \mathrm{SR}\{V_{i,j,t}\}$$

The CO_2 fertilisation effect as a function of NDVI shows saturation at high values because of the non-linear relationship between NDVI and SR.

Time series of mean annual values over 1901–2010 for both adjusted CCVI and CO_2 adjusted CCVI are shown in Fig. 6. Note that filled (close to zero) values were not included in the CCVI global average but were included in the previously reported RVI average (Los, 2013). The increase in global mean CCVI compared to RVI over the 20th century is similar for the CO_2 fertilised scenarios, but is smaller in the CCVI compared to the RVI when CO_2 fertilisation is not included.

4 Results: testing and analysing the CCVI

Spatial correlations (Sect. 4.1), seasonal correlations and interannual correlations (Sect. 4.2) were calculated between CCVI on the one hand and NDVI or RVI on the other. Interannual variations in CCVI were also compared with phenology data, mostly

GMDD
8, 4781–4821, 2015

for the latter part of the 20th century (Sect. 4.3). The response of the CCVI to two known extreme events was explored; the dust bowl in North America during the 1930s and 1950s, and the drought of the century in the Sahel south of the Sahara in 1984 (Sect. 4.4). The response of the CCVI to climate change scenarios was compared with the leaf seasonality simulations from three Earth System Models (Sect. 4.5).

4.1 Spatial correlation

Figure 7 shows monthly spatial correlations over time between FASIR NDVI on the one hand and RVI, CCVI (control) and CCVI adjusted for bias on the other. The RVI shows the highest spatial correlations, the adjusted CCVI the next highest and the CCVI control the lowest. The RVI is tuned to the observed time series of a particular cell (Los, 2013) and this tends to underestimate or diminish the effect of errors in the RVI that should be present as a result of errors in spatial interpolation of precipitation or temperature.

Spatial correlations are on average higher for 1982–1999 because data from this period were used to derive both the RVI and CCVI models. A large decrease appears in the spatial correlation for the RVI between the AVHRR (1982–1999) and MODIS period (2000–2010); this decrease is more gradual in the CCVI. Potential causes for the decrease in spatial correlation after 2000 are (1) that the quality of gridded precipitation and temperature data diminishes over time as a result of a decrease in the number of observations available, (2) differences between the MODIS and AVHRR NDVI or (3) both. A minor but interesting feature can be observed in the spatial correlations for the CCVI; these correlations exhibit a saw tooth pattern with higher correlations just after launch of subsequent NOAA satellites and a decrease during their time of operation; thus correlations decrease from 1982–1985 (NOAA-7), from 1985–1989 (NOAA-9), from 1990–1995 (NOAA-11) and from 1995–1999 (NOAA-14). This feature can be linked to the gradual drift in overpass time to later times of the day and residual BRDF effects (Los, 1998a; Los et al., 2005).

GMDD
8, 4781–4821, 2015

4.2 Temporal correlation

Both seasonal and interannual temporal correlations were calculated between FASIR NDVI on the one hand and RVI and CCVI on the other. Seasonal correlations with FASIR NDVI were high for both RVI and CCVI for 1982–1999, the period from which equations were derived, and for 2001–2006; the period not used for model development (Fig. 9). The CCVI showed low correlations in areas with small seasonal variations such as as in deserts and tropical forests. Correlations for RVI in these areas were high; the small variability in NDVI in these areas may not be related to vegetation, however, but can be associated with other factors such as variations in atmospheric water vapour over the Sahara (Holben, 1986).

Temporal correlations for anomalies in RVI were high for 1982–1999 but lower for 2001–2006. Areas with high interannual variability (semi arid regions and temperate regions) showed higher correlations. The CCVI showed lower correlations for 1982–1999 than the RVI but higher correlations for 2001–2006 indicating greater skill in predicting interannual variations for periods not used to derive the model.

The correlations between RVI control and CCVI control anomalies (the control was used to reduce the effect of trends associated with CO_2 fertilisation on correlations) were compared for the periods of 1901–1981, 1982–1999, 2001–2006 and 1982–2006 (Fig. 10). Most areas of high interannual variability showed high correlations between RVI and CCVI.

4.3 Phenology time series

Figure 11 shows frequency distributions of correlations between either the leaf out date or the first day of bloom with CCVI. Phenology data were obtained for lilac leaf out and bloom in North America (Schwartz and Reiter, 2000; Schwartz and Caprio, 2003), Oak in Germany (data provided by the German weather service), Cherry Blossom Russia (from http://www.biodat.ru/) and the Marsham oak time series from the UK (Sparks and Carey, 1995). The correlations are the maximum correlations for the month previous to the day of leaf out, the month concurrent with the day of leaf out, or the month after the day of leaf out. The frequency distributions showed more significant (larger negative) correlations for the CCVI in the German oak and cherry bloom cases than for RVI. RVI and CCVI correlations were similar for the lilac data. The Marsham oak correlation 1901–1958 was −0.41 fore CCVI vs. −0.78 for the RVI (Los, 2013). Overall the CCVI captured interannual variation in the phenology data better than the RVI.

4.4 Extreme events

Over the course of the 20th century extreme events occurred that had a severe negative impact on vegetation. Two well-known examples are the drought in and around the Great Plains in North America, referred to as the dust bowls of the 1930s and 1950s, and the drought of the century in the Sahel in 1984. Figure 12a shows the mean annual RVI and CCVI times series for an area in the Great Plains. Both time series show a decrease in values during the 1930s and the CCVI also shows a decrease during the 1950s. The NPP calculated by the CENTURY model (Metherall et al., 1993) by comparison does not show any significant decrease during these periods (Fig. 12b). The CENTURY model uses a different leaf phenology model that, for this case, fails to capture the effects of drought on vegetation. The precipitation data for the same area indicate a decrease during the 1930s and a smaller decrease during the 1950s similar to the decrease in the CCVI.

The time series of RVI and CCVI for an area in the Sahel, the second drought example, are shown in Fig. 12c. Both time series show a decrease in values during 1984 and both match the NDVI data from 1982–2010 well. Correlations between RVI and precipitation are higher than correlations between CCVI and precipitation (Fig. 12).

4.5 Comparison CCVI with leaf area index from climate change scenarios

The CCVI was calculated for three climate change scenarios to explore differences with current implementations of leaf seasonality models. The three climate change scenarios were obtained for the representative concentration pathway RCP4.5 for 2006–2100 (Thomson et al., 2011) and were from the MPI-ESM (Giorgetta et al., 2013) coupled to the JSBACH/BETHY land-surface parameterisation (Raddatz et al., 2007), the Hadgem-CC model (Collins et al., 2011) coupled to MOSES TRIFFID (Clark et al., 2011) and the CESM model coupled to the BioGeochemical Cycles model (CESM1-BGC) (Kay et al., 2014). The scenarios form part of the coupled model intercomparison project phase 5 (Taylor et al., 2012). Precipitation and surface air surface temperature from 2046–2075 were used to calculate the KT classes, and $CCVI_{CO_2}$ was calculated for 2006–2100 using precipitation surface air temperature and the RCP4.5 mid-year greenhouse gas concentrations for 2006–2100 (Meinshausen et al., 2011). The comparison with leaf area index was made for the last 30 years of the simulations; during this period the CO_2 concentrations have stabilised for RCP4.5 which excludes trend effects from the analysis.

Figure 13a shows the change in LAI between two 15 year periods calculated as the average for 2086–2100 minus the average for 2071–2085 for the CESM1-BGC model. Figure 13b and c show the partial correlation between leaf area index and temperature and precipitation respectively. Temperature shows large negative correlations for most of the tropics and positive correlations for high northern latitudes. Partial correlations with precipitation are low in general. Figure 13d shows the difference between the last two 15 year periods in CCVI. Differences tend to be smaller in the tropics, but larger in mid to high latitudes compared to the change in LAI. Correlations with temperature are negative in the tropics and appear of similar magnitude as correlations for LAI; however, positive correlations with temperature appear high throughout most of the mid-to-high latitudes. Correlations with precipitation are higher across the globe compared to correlations with LAI. Results for the other two climate models, provided in the Supplement, show substantially higher partial correlations between CCVI precipitation than for LAI and precipitation for mid latitudes as well. As an aside, notice that the UK Met Office model shows no change in the LAI over the Amazon and that correlations between LAI and both temperature and precipitation are low. Overall, the

GMDD
8, 4781–4821, 2015

CCVI appears more sensitive to variations in precipitation in mid latitudes than current implementations of leaf seasonality models.

5 Discussion

The aim of the present study was to develop a model that predicts global spatial, seasonal and interannual variations in the normalised difference vegetation index for a range of climates. The resulting model, referred to as the climate constrained vegetation index (CCVI) required only atmospheric CO_2 concentrations, precipitation and temperature as input; climate vs. NDVI relationship depended on a stratification of the globe into the 6 Köppen–Trewartha classes A–F, but other eco-climatic classification systems could be used in lieu of the KT classification. Biophysical parameters such as LAI or the fraction of photosynthetically active radiation absorbed by green parts of the vegetation canopy can be estimated similar to the approach adopted for the CCVI or can be estimated from the CCVI (Sellers et al., 1996; Los et al., 2000). Implementation of the CCVI using a hydrological model was not considered since in a previous study only a minor improvement was found for one land-surface model and worse performance for two others (Los, 2015).

Constraints on the NDVI were calculated for each of the KT classes as the minimum of 7 precipitation functions at different lags and 5 temperature functions at different lags; separate functions were derived for increasing and decreasing NDVI. The constraint functions provided evidence of adaptations of vegetation to different climate regimes. The adaptations of vegetation to colder climates were particularly prominent. NDVI values around freezing point increased with decreasing average temperature for a KT zone; thus NDVI at freezing for class F > class E > class D > class C. This differentiation according to climate zone is not found in the Miami model which uses one equation to calculate temperature constraints on annual NPP across the globe. The higher NDVI values at low temperatures for colder climates will result in more realistic, lower albedo estimates which is of importance for the calculation of the energy budget and of land-surface temperatures (Betts and Ball, 1997; Betts et al., 2001). Other processes will also be affected by higher NDVI values at low temperatures, such as photosynthesis, net primary productivity and the interception of precipitation.

The CCVI model captured spatial, seasonal and interannual variations well; spatial correlations were lower than for the previously developed RVI. Some of the seasonal and spatial variability captured in the RVI may not be present in the source data (precipitation and temperature), and therefore the RVI may underestimate errors. Further evidence of this is that the CCVI picks up residual BRDF errors in the FASIR NDVI, which the RVI does not.

Compared to other land-surface schemes the CCVI had higher spatial correlation; monthly spatial correlations globally between CCVI and NDVI varied between 0.8 and 0.87; for latitudes above 30° N average spatial correlation varied around 0.75; which is higher than spatial correlations for current leaf seasonality models which vary between 0.2–0.66 (Anav et al., 2013).

Seasonal variations were similarly high for both RVI and CCVI in areas with large vegetation seasonality. The CCVI did not capture seasonal variations in NDVI as well as the RVI over areas with small seasonal amplitudes such as deserts and tropical forests. However, NDVI seasonality in these areas is not always linked to variability in vegetation and deviations from observed values were often small.

Interannual variations outside the period used for model development were overall better captured by the CCVI than the RVI. The global median correlation for CCVI interannual variability was around 0.24; this number includes areas with low temporal variability (but not deserts or tropical forests). Since the interannual signal in NDVI is small, in the order of 0.1 NDVI, and residual errors can be in the range of 0.05 NDVI and r value of at best 0.7 can be expected. Very few studies provide tests of interannual variability for leaf area index or associated parameters. The study by Gibelin et al. (2006) using the Interactions between Soil, Biosphere and Atmosphere (ISBA) calibrated interannual variability in LAI to observations. Correlations of interannual variability in ISBA LAI were similar to those found in the the present study (see Gibelin et al.

GMDD
8, 4781–4821, 2015

(2006), Fig. 3). The analysis of two extreme events, the dust bowl and Sahel, shows that the CCVI captures the effects of droughts.

The CCVI resulted in larger interannual variability in vegetation in response to climate variability than implementations in (at least three) current earth system/general circulation models. In particular, the greater sensitivity of vegetation towards drought and temperature is important to capture in land-surface parameterisations. A recent analysis of a range of climate change scenarios indicated possible drying or more frequent droughts (Polade et al., 2014). The present analysis indicates that current land-surface parameterisations underestimate the response of vegetation to drought and therefore underestimate the implications for, e.g. agriculture. A recent study presents observational evidence that the relationship between NDVI and temperature switched from a positive to a negative relationship for a large region around the Ural mountains, this switch could possibly be linked to increased drought stress (Buermann et al., 2014).

The effect of CO_2 fertilisation appeared of similar magnitude as an earlier estimate. The magnitude of the effect increased linearly with simple ratio; a transformation of the NDVI. This allows for a straightforward implementation in models and provides an estimate valid at regional to continental scale.

6 Conclusions

(1) The constraint analysis showed higher low temperature tolerance in vegetation of colder climatic zones – at freezing, the NDVI of class E was about 0.2 NDVI higher than of Class C; this adaptation is not implemented in some vegetation models. (2) Realistic spatial and temporal estimates of NDVI, here referred to as CCVI, were obtained from precipitation and temperature constraints. The previously developed RVI (Los, 2013) exhibited more realistic spatial variability, however, the CCVI demonstrated greater skill in predicting interannual variability. Moreover, the CCVI can be applied to a wider range of climates than the RVI. (3) Implementation of the CCVI in land-surface parameterisations and ecosystem models is straightforwards since only temperature,

GMDD
8, 4781–4821, 2015

Title Page
Abstract Introduction
Conclusions References
Tables Figures
◀◀ ▶▶
◀ ▶
Back Close
Full Screen / Esc
Printer-friendly Version
Interactive Discussion

precipitation and atmospheric CO_2 concentrations are required as inputs. Inclusion of a water balance model was not considered given the relatively poor performance of hydrological schemes in land-surface parameterisations (Los, 2015). (4) The CCVI showed greater sensitivity towards variations in climate, in particular to change in precipitation in continental interiors, than leaf seasonality schemes implemented in land-surface parameterisations investigated. The ability to reproduce the manifestation of drought in vegetation is of great importance for estimation of the effects of climate variability on vegetation, and is particularly important to assess risks for crop productivity. (5) The magnitude of CO_2 the fertilisation effect on global NDVI found in an earlier study (Los, 2013) was confirmed; the magnitude of the effect was found to change linearly with simple ratio.

Code availability

The code is written in the R language (http://www.r-project.org) and is available upon request from the author (s.o.los@swansea.ac.uk). An implementation of the model in Fortran is under development.

The Supplement related to this article is available online at doi:10.5194/gmdd-8-4781-2015-supplement.

Acknowledgements. CRU TS version 3.21 precipitation data and temperature data and the Hadgem-CC, CESM1-BGC and MPI-ESM-MR RCP4.5 realisation 1 precipitation, temperature and leaf area index simulations were obtained from the British Atmospheric Data Centre (BADC; http://badc.nerc.ac.uk/). The RCP4.5 atmospheric CO_2 concentrations were obtained from the Potsdam institute for Climate Impact Research (http://www.pik-potsdam.de/). The Deutscher Wetterdienst (German Meteorological Service) provided the German oak data; M. Schwartz and J. Caprio provided the North American lilac phenology data through the

NOAA NCDC Paleoclimatology Program; T. Sparks (CEH) and I. Robertson (Swansea University) provided the Marsham oak data; A. Andreevitch provided the Russian Bird Cherry data (http://www.biodat.ru/); and P. Tans and C. Keeling provided the Mauna Loa CO_2 data through the NOAA ESRL.

References

Anav, A., Murray-Tortarolo, G., Friedlingstein, P., Sitch, S., Piao, S., and Zhu, Z.: Evaluation of land-surface models in reproducing satellite-derived leaf area index over the high-latitude Northern Hemisphere. Part II: Earth system models, Remote Sensing, 5, 3637–3661, 2013. 4783, 4797

Beljaars, A. C. M., Viterbo, P., Miller, M. J., and Betts, A. K.: The anomalous rainfall over the United States during July 1993: sensitivity to land surface parameterization and soil moisture anomalies, Mon. Weather Rev., 124, 362–382, 1996. 4782

Best, M. J., Pryor, M., Clark, D. B., Rooney, G. G., Essery, R. L. H., Ménard, C. B., Edwards, J. M., Hendry, M. A., Porson, A., Gedney, N., Mercado, L. M., Sitch, S., Blyth, E., Boucher, O., Cox, P. M., Grimmond, C. S. B., and Harding, R. J.: The Joint UK Land Environment Simulator (JULES), model description – Part 1: Energy and water fluxes, Geosci. Model Dev., 4, 677–699, doi:10.5194/gmd-4-677-2011, 2011. 4783

Betts, A. K. and Ball, J. H.: Albedo over the boreal forest, J. Geophys. Res., 102, 28901–28909, 1997. 4797

Betts, A. K., Viterbo, P., Beljaars, A. C. M., and van den Hurk, B. J. J. M.: Impact of BOREAS on the ECMWF forecast model, J. Geophys. Res., 106, 33593–33604, doi:10.1029/2001JD900056, 2001. 4797

Buermann, W., Parida, B., Jung, M., MacDonald, G. M., Tucker, C. J., and Reichstein, M.: Recent shift in Eurasian boreal forest greening response may be associated with warmer and drier summers, Geophys. Res. Lett., 41, 1995–2002, doi:10.1002/2014GL059450, 2014. 4798

Clark, D. B., Mercado, L. M., Sitch, S., Jones, C. D., Gedney, N., Best, M. J., Pryor, M., Rooney, G. G., Essery, R. L. H., Blyth, E., Boucher, O., Harding, R. J., Huntingford, C., and Cox, P. M.: The Joint UK Land Environment Simulator (JULES), model description – Part 2:

GMDD

8, 4781–4821, 2015

Carbon fluxes and vegetation dynamics, Geosci. Model Dev., 4, 701–722, doi:10.5194/gmd-4-701-2011, 2011. 4783, 4795

Collins, W. J., Bellouin, N., Doutriaux-Boucher, M., Gedney, N., Halloran, P., Hinton, T., Hughes, J., Jones, C. D., Joshi, M., Liddicoat, S., Martin, G., O'Connor, F., Rae, J., Senior, C., Sitch, S., Totterdell, I., Wiltshire, A., and Woodward, S.: Development and evaluation of an Earth-System model – HadGEM2, Geosci. Model Dev., 4, 1051–1075, doi:10.5194/gmd-4-1051-2011, 2011. 4785, 4795

Dickinson, R. E., Oleson, K. W., Bonan, G., Hoffman, F., Thornton, P., Vertenstein, M., Yang, Z. L., and Zeng, X.: The Community Land Model and its climate statistics as a component of the Community Climate System Model, J. Climate, 19, 2302–2324, doi:10.1175/JCLI3742.1, 2006. 4783

Esser, G., Hoffstadt, J., Mack, F., and Wittenberg, U.: High Resolution Biosphere Model, Model Version 3.00.00, Tech. rep., Institute for Plant Ecology, Justus-Liebig Universität, Giessen, Germany, 1994. 4783, 4809

Etheridge, D. M., Steele, L. P., Langenfelds, R. L., Francey, R. J., Barnola, J. M., and Morgan, V. I.: Law Dome atmospheric CO_2 data, Tech. rep., IGBP PAGES/World Data Center for Paleoclimatology, Data Contribution Series # 2001-083, NOAA/NGDC Paleoclimatology Program, Boulder CO, USA, 2001. 4785

Gibelin, A., Calvet, J., Roujean, J., Jarlan, L., and Los, S. O.: Ability of the land surface model ISBA-A-gs to simulate leaf area index at the global scale: comparison with satellites products, J. Geophys. Res., 111, D18102, doi:10.1029/2005JD006691, 2006. 4797

Giorgetta, M. A., Jungclaus, J., Reick, C. H., Legutke, S., Bader, J., Böttinger, M., Brovkin, V., Crueger, T., Esch, M., Fieg, K., Glushak, K., Gayler, V., Haak, H., Hollweg, H.-D., Ilyina, T., Kinne, S., Kornblueh, L., Matei, D., Mauritsen, T., Mikolajewicz, U., Mueller, W., Notz, D., Pithan, F., Raddatz, T., Rast, S., Redler, R., Roeckner, E., Schmidt, H., Schnur, R., Segschneider, J., Six, K. D., Stockhause, M., Timmreck, C., Wegner, J., Widmann, H., Wieners, K.-H., Claussen, M., Marotzke, J., and Stevens, B.: Climate and carbon cycle changes from 1850 to 2100 in MPI-ESM simulations for the Coupled Model Intercomparison Project phase 5, J. Adv. Model. Earth Sy., 5, 572–597, doi:10.1002/jame.20038, 2013. 4785, 4795

Harris, I., Jones, P. D., Osborn, T. J., and Lister, D. H.: Updated high-resolution grids of monthly climatic observations – the CRU TS3.10 Dataset, Int. J. Climatol., 34, 623–712, doi:10.1002/joc.3711, 2014. 4785

Haxeltine, A. and Prentice, I. C.: BIOME3: an equilibrium terrestrial biosphere model based on eco-physiological constraints, resource availability, and competition among plant functional types, Global Biogeochem. Cy., 10, 693–709, 1996. 4783

Holben, B. N.: Characteristics of maximum-value composite images from temporal AVHRR data, Int. J. Remote Sens., 7, 1417–1434, 1986. 4793

James, M. E. and Kalluri, S. N. V.: The Pathfinder AVHRR land data set – an improved coarse resolution data set for terrestrial monitoring, Int. J. Remote Sens., 15, 3347–3363, 1994. 4785

Kay, J. E., Deser, C., Phillips, A., Mai, A., Hannay, C., Strand, G., Arblaster, J., Bates, S., Danabasoglu, G., Edwards, J., Holland, M., Kushner, P., Lamarque, J., Lawrence, D., Lindsay, K., Middleton, A., Munoz, E., Neale, R., Oleson, K., Polvani, L., and Vertenstein, M.: The Community Earth System Model (CESM) large ensemble project: a community resource for studying climate change in the presence of internal climate variability, B. Am. Meteorol. Soc., in press, doi:10.1175/BAMS-D-13-00255.1, 2014. 4785, 4795

Keeling, C. D., Bacastow, R. B., Bainbridge, A. E., Ekdahl, C. A., Guenther, P. R., and Waterman, L. S.: Atmospheric carbon dioxide variations at Mauna Loa Observatory, Hawaii, Tellus, 28, 538–551, 1976. 4785

Knorr, W., Kaminski, T., Scholze, M., Gobron, N., Pinty, B., Giering, R., and Mathieu, P. P.: Carbon cycle data assimilation with a generic phenology mode, J. Geophys. Res., 115, G04017, doi:10.1029/2009JG001119, 2010. 4783, 4784

Lieth, H.: Modelling primary productivity of the world, in: Primary Productivity of the Biosphere, Ecological Studies 14, Springer Verlag, Berlin, Heidelberg, New York, 237–263, 1975. 4783, 4784, 4787, 4809

Los, S. O.: Calibration adjustment of the NOAA Advanced Very High Resolution Radiometer without recourse to component channel-1 and channel-2 data, Int. J. Remote Sens., 14, 1907–1917, 1993. 4785

Los, S. O.: Linkages between global vegetation and climate: an analysis based on NOAA Advanced Very High Resolution Radiometer data, PhD thesis, Vrije Universiteit Amsterdam, the Netherlands, 1998a. 4792

Los, S. O.: Estimation of the ratio of sensor degradation between NOAA AVHRR channels 1 and 2 from monthly NDVI composites, IEEE T. Geosci. Remote, 36, 206–213, doi:10.1109/36.655330, 1998b. 4785

Los, S. O.: Analysis of trends in fused AVHRR and MODIS NDVI data for 1982–2006: IIndication for a CO2 fertilization effect in global vegetation, Global Biogeochem. Cy., 27, 318–330, doi:10.1002/gbc.20027, 2013. 4783, 4784, 4785, 4790, 4791, 4792, 4794, 4798, 4799, 4816, 4819

Los, S. O.: Testing gridded land precipitation data and precipitation and runoff reanalyses (1982–2010) between 45° S and 45° N with normalised difference vegetation index data, Hydrol. Earth Syst. Sci., 19, 1713–1725, doi:10.5194/hess-19-1713-2015, 2015. 4783, 4787, 4796, 4799

Los, S. O., Collatz, G. J., Sellers, P. J., Malmstrom, C. M., Pollack, N. H., DeFries, R. S., Bounoua, L., Parris, M. T., Tucker, C. J., and Dazlich, D. A.: A global 9-yr biophysical land surface data set from NOAA AVHRR data, J. Hydrometeorol., 1, 183–199, 2000. 4785, 4796

Los, S. O., North, P. R. J., Grey, W. M. F., and Barnsley, M. J.: A method to convert AVHRR Normalized Difference Vegetation Index time series to a standard viewing and illumination geometry, Remote Sens. Environ., 99, 400–411, doi:10.1016/j.rse.2005.08.017, 2005. 4785, 4790, 4792

Los, S. O., Weedon, G. P., North, P. R. J., Kaduk, J. D., Taylor, C. M., and Cox, P. M.: An observation-based estimate of the strength of rainfall–vegetation interactions in the Sahel, Geophys. Res. Lett., 33, L16402, doi:10.1029/2006GL027065, 2006. 4782, 4783, 4784

Los, S. O., Hancock, S., North, P., and Gomez-Dans, J.: Improved vegetation phenology in the JULES land-surface model, AGU Conference, San Francisco, American Geophys. Union, 09–13 December 2013, 2013 AGUFM.B53F.08L, 2013. 4783

Loveland, T. R., Reed, B. C., Brown, J. F., Ohlen, D. O., Zhu, J., Yang, L., and Merchant, J. W.: Development of a global land cover characteristics database and IGBP DISCover from 1-km AVHRR Data, Int. J. Remote Sens., 21, 1303–1330, 2001. 4787, 4807

Malmström, C., Thompson, M., Juday, G., Los, S., Randerson, J., and Field, C.: Interannual variation in global-scale net primary production: testing model estimates, Global Biogeochem. Cy., 11, 367–392, 1997. 4783, 4787

Meinshausen, M., Smith, S., Calvin, K., Daniel, J. S., Kainuma, M. L. T., Lamarque, J., Matsumoto, K., Montzka, S. A., Raper, S. C. B., Riahi, K., Thomson, A., Velders, G. J. M., and van Vuuren, D. P. P.: The RCP GHG concentrations and their extension from 1765 to 2300, Climatic Change, 109, 213–241, doi:10.1007/s10584-011-0156-z, 2011. 4786, 4795

Metherall, A. K., Harding, L. A., Cole, C. V., and Parton, W. J.: CENTURY Soil Organic Matter Model Environment Technical Documentation, Agroecosystem Version 4.0, Great Plains System Research Unit, USDA-ARS, Fort Collins, Colorado, USA, 1993. 4783, 4794, 4820

Muggeo, V. M. R.: Estimating regression models with unknown break-points, Stat. Med., 22, 3055–3071, 2003. 4788, 4810

Muggeo, V. M. R.: Segmented: an R package to fit regression models with broken-line relationships, R News, available at: http://cran.r-project.org/doc/Rnews/ (last access: 19 June 2015), 8, 20–25, 2008. 4788, 4810

Polade, S. J., Pierce, D. W., Cayan, D. R., Gershunov, A., and Dettinger, M. D.: The key role of dry days in changing regional climate and precipitation regimes, Sci. Rep., 4, 4364, doi:10.1038/srep04364, 2014. 4798

Potter, C. S., Randerson, J. T., Field, C. B., Matson, P. A., Vitousek, P. M., Mooney, H. A., and Klooster, S. A.: Terrestrial ecosystem production: a process model based on global satellite and surface data., Global Biogeochem. Cy., 7, 811–841, 1993. 4784

Raddatz, T. J., Reick, C. H., Knorr, W., Kattge, J abd Roeckner, E., Schnur, R., Schnitzler, K., Wetzel, P., and Jungclaus, J.: Will the tropical land biosphere dominate the climate-carbon cycle feedback during the twenty first century?, Clim. Dynam., 29, 565–574, doi:10.1007/s00382-007-0247-8, 2007. 4795

Randerson, J. T., Hoffman, F. M., Thornton, P. E., Mahowals, N. M., Lindsay, K., Lee, Y. H., Nevison, C. D., Doney, S. C., Bonan, G. B., Stöckli, R., Covey, C., Running, S. W., and Fung, I. Y.: Systematic assessment of terrestrial biogeochemistry in coupled climate–carbon models, Glob. Change Biol., 15, 2462–2484, doi:10.1111/j.1365-2486.2009.01912.x, 2009. 4783

Richardson, A. D., Anderson, R. S., Arain, M. A., Barr, A. G., Bohrer, G., Chen, G., Chen, J. M., Ciais, P., Davis, K. J., Desai, A. R., Dietze, M. C., Dragoni, D., Garrity, S. R., Gough, C. M., Grant, R., Hollinger, D. Y., Margolis, H. A., McCaughey, H., Migliavacca, M., Monson, R. K., Munger, J. W., Poulter, B., Raczka, B. M., Ricciuto, D. M., Sahoo, A. K., Schaefer, K., Tian, H., Vargas, R., Verbeeck, H., Xiao, J., and Xue, Y.: Terrestrial biosphere models need better representation of vegetation phenology: results from the North American Carbon Program Site Synthesis, Glob. Change Biol., 18, 566–584, doi:10.1111/j.1365-2486.2011.02562.x, 2012. 4783

Rousseeuw, P. J. and Leroy, A. M.: Robust Regression and Outlier Detection, Wiley, New York, 1987. 4791

GMDD

8, 4781–4821, 2015

Climate related variability in vegetation greenness

S. O. Los

Schwartz, M. D. and Caprio, J. M.: North American First Leaf and First Bloom Lilac phenology data, Tech. rep., IGBP PAGES/World Data Center for Paleoclimatology, NOAA/NGDC Paleoclimatology program, Boulder, Colorado, USA, 2003. 4793

Schwartz, M. D. and Reiter, B. E.: Change in North American spring, Int. J. Climatol., 20, 929–932, 2000. 4793

Sellers, P. J., Los, S. O., Tucker, C. J., Justice, C. O., Dazlich, D. A., Collatz, G. J., and Randall, D. A.: A revised land-surface parameterization (SiB2) for Atmospheric GCMs. Part 2: The generation of global fields of terrestrial biophysical parameters from satellite data, J. Climate, 9, 706–737, 1996. 4784, 4785, 4796, 4807

Sitch, S., Smith, B., Prentice, I. C., Arneth, A., Bondeau, A., Cramer, W., Kaplans, J. O., Levis, S., Lucht, W., Sykes, M. T., Thonicke, K., and Venevsky, S.: Evaluation of ecosystem dynamics, plant geography and terrestrial carbon cycling in the LPJ dynamic global vegetation model, Glob. Change Biol., 9, 161–185, 2003. 4783

Sparks, T. H. and Carey, P. D.: The responses of species to climate over two centuries: an analysis of the Marsham phenological record, 1736–1947, J. Ecol., 83, 321–329, 1995. 4793, 4819

Taylor, C. M. and Ellis, R. J.: Satellite detection of soil moisture impacts on convection at the mesoscale, Geophys. Res. Lett., 33, L03404, doi:10.1029/2005GL025252, 2006. 4782

Taylor, K. E., Stouffer, R. J., and Meehl, G. A.: An overview of CMIP5 and the experimental design, B. Am. Meteorol. Soc., 93, 485–498, doi:10.1175/BAMS-D-11-00094.1, 2012. 4785, 4795

Thomson, A. M., Calvin, K. V., Smith, S. J., Kyle, G. P., Volke, A., Patel, P., Delgado-Arias, S., Bond-Lamberty, B., Wise, M. A., Clarke, L. E., and Edmonds, J. A.: RCP4.5: a pathway for stabilization of radiative forcing by 2100, Climatic Change, 109, 77–94, doi:10.1007/s10584-011-0151-4, 2011. 4795

Thoning, K. W., Tans, P. P., and Komhyr, W. D.: Atmospheric carbon dioxide at Mauna Loa Observatory 2. Analysis of the NOAA GMCC data, 1974–1985, J. Geophys. Res., 94, 8549–8565, 1989. 4785

Trewartha, G. T. and Sale, R. D.: An Introduction to Climate, McGraw-Hill, New York, Maindenhead, 1968. 4784

Vermote, E. F., Justice, C. O., Descloitres, J., El Saleous, N., Roy, D. P., Ray, J., Margerin, B., and Gonzalez, L.: A SeaWiFS global monthly coarse-resolution reflectance data set, Int. J. Remote Sens., 22, 1151–1158, 2001. 4785

GMDD
8, 4781–4821, 2015

Climate related variability in vegetation greenness

S. O. Los

Table 1. Köppen–Trewartha classification rules with T_{min} the minimum average monthly temperature over 30 years; $R = 2.3T_{avg} - 0.64P_w + 41$. T_{avg} the average annual surface air temperature over 30 years, P_w is the winter precipitation, here taken as November until April (inclusive) for the Northern Hemisphere and April until September (inclusive) for the Southern Hemisphere; $N_{T>10} = \sum_{i=1}^{360}(T_i > 10)/30$ is the total number of months mean temperature above 10 °C during a 30 year period divided by 30. $N_{T>10}$ is used as a continuous variable, rather than an integer variable as is the case in the KT classification. Thresholds based on $N_{T>10}$ that identify class boundaries have been revised as well.

KT Class	Threshold
A	$T_{min} > 18$
BS	$R/2 \le P_{avg} < R$
B	$P_{avg} < R/2$
C	$N_{T>10} > 7.5$
D	$7.5 \ge N_{T>10} > 3.5$
E	$3.5 > N_{T>10} \ge 0.5$
F	$N_{T>10} < 0.5$

Table 2. Matrix comparing agreement between Köppen–Trewartha classes and USGS-EDC SiB Classes (Loveland et al., 2001; Sellers et al., 1996). Numbers indicate percentage of total land surface between 60° S and 80° N; percentages > 1 % are in bold face. Wetlands (EDC SiB class 13) are excluded, permanent snow and ice (EDC SiB class 14) is considered bare soil.

KT Class/SiB Class		A	BS	B	C	D	E	F
1	Evergreen broad leaf trees	**8.790**	0.089	0.002	0.956	0.186	0.089	0.016
2	Broad leaf deciduous trees	0.035	0.004	0.002	0.144	**1.050**	**1.170**	0.016
3	Deciduous and evergreen trees	0.158	0.049	0.000	0.734	**1.530**	0.755	0.001
4	Evergreen needle leaf trees	0.209	0.059	0.000	0.502	**1.830**	**3.310**	0.022
5	Deciduous needle leaf trees	0.000	0.000	0.000	0.000	0.286	**2.500**	0.008
6	Trees with ground cover	**5.300**	**5.940**	**1.600**	**3.120**	0.488	0.339	0.007
7	Ground cover	0.007	0.538	**1.230**	0.318	**2.200**	0.406	0.039
8	Shrubs with ground cover	0.018	0.416	**1.580**	0.323	0.281	0.547	0.122
9	Shrubs and bare soil	0.000	**1.100**	**4.050**	0.167	**2.530**	0.281	0.683
10	Tundra	0.028	0.118	0.1330	0.037	0.693	**4.200**	**2.640**
11	Bare soil	0.002	0.310	**9.760**	0.024	**1.270**	0.168	**2.363**
12	Agriculture	**2.130**	**2.460**	0.549	**3.870**	**9.100**	0.722	0.636

GMDD
8, 4781–4821, 2015

Climate related variability in vegetation greenness

S. O. Los

Table 3. Variables for which climate constraints on NDVI were derived. P is total precipitation, T is mean monthly temperature, V is CCVI during calculations or NDVI for initial estimates, t is month for which end-of-month CCVI values were estimated.

Lag (month)	Precipitation	Temperature	NDVI (min constraint)
0	${}^{10}\log\{P_t+1\}$	T_t	
1	${}^{10}\log\{P_{t-1}+1\}$	T_{t-1}	
2	${}^{10}\log\{P_{t-2}+1\}$	T_{t-2}	
0–1	${}^{10}\log\{P_t+P_{t-1}+1\}$	$\sum_{i=0}^{1}T_{t-i}/2$	
0–2	${}^{10}\log\{P_t+P_{t-1}+P_{t-2}+1\}$	$\sum_{i=0}^{2}T_{t-i}/3$	
0–3	${}^{10}\log\{P_t+P_{t-1}+P_{t-2}+P_{t-3}+1\}$		
0–11	${}^{10}\log\{\sum_{i=0}^{11}P_{t-i}+1\}$		$0.05\sum_{i=1}^{12}V_{t-i}$

GMDD
8, 4781–4821, 2015

Climate related variability in vegetation greenness

S. O. Los

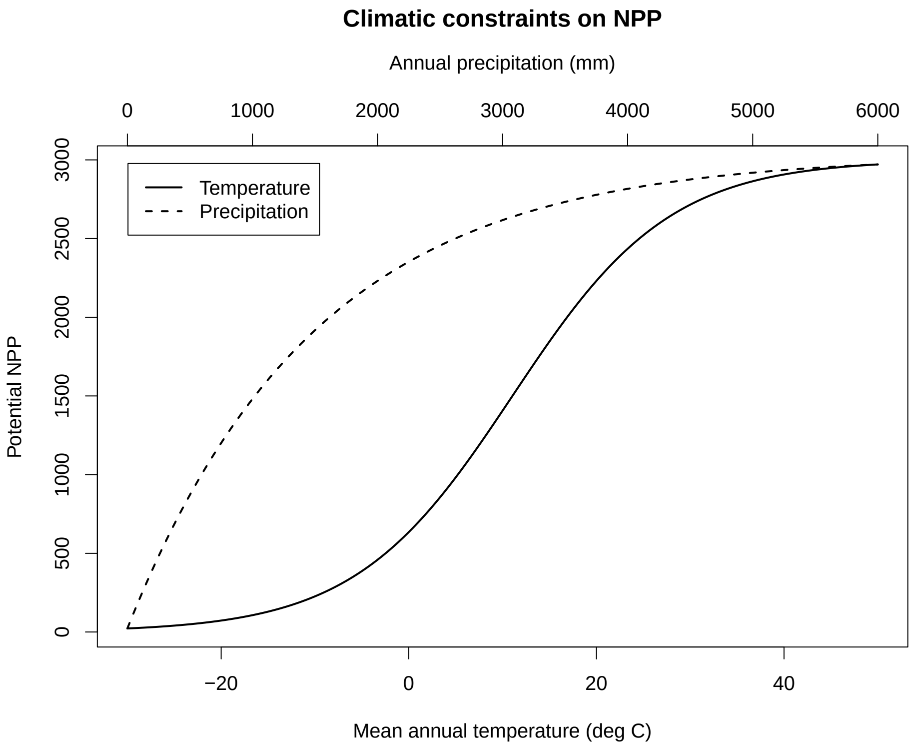

Figure 1. Climate (mean annual temperature – x axis at the bottom, continuous line – and total annual precipitation – x axis at the top, dashed line) constraints on potential annual net primary productivity (NPP) according to the Miami model (Lieth, 1975; Esser et al., 1994). The temperature constraint on NPP is given by $\mathrm{NPP}_T = 3000/(1+\exp(1.315-0.197T))$ with T the mean annual temperature (°C), and the precipitation constrain is given by $\mathrm{NPP}_P = 3000 \times (1 - \exp(-0.000664P))$ with P the total annual precipitation ($\mathrm{mm\,yr^{-1}}$).

GMDD
8, 4781–4821, 2015

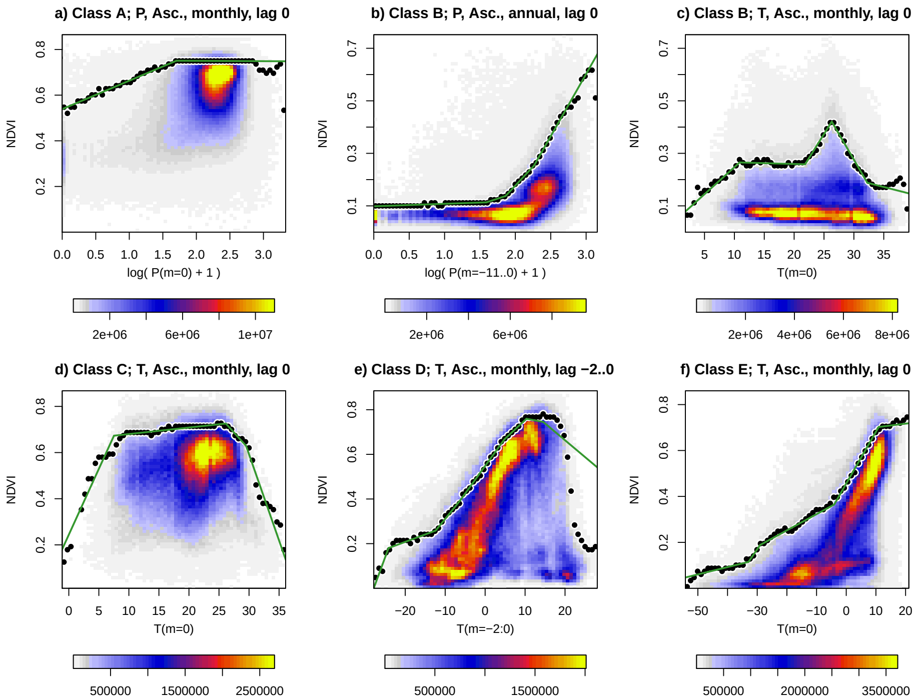

Figure 2. Example derivations of temperature and precipitation constraints on monthly NDVI; relationships are for ascending NDVI. **(a)** End-of-month NDVI as a function of monthly precipitation for KT class A; the dots show the 95th percentile for each of 64 intervals and the green line shows the fit through these dots as estimated with segmented regression (Muggeo, 2003, 2008). **(b)** End of month NDVI as a function of *annual* precipitation for KT class B. (**c** and **d**) End of month NDVI as a function of monthly temperature for KT class B and C, respectively. **(e)** End of month NDVI (KT class D) as a function of mean temperature for the current and past two months. **(f)** As (**c** and **d**); but for KT class E.

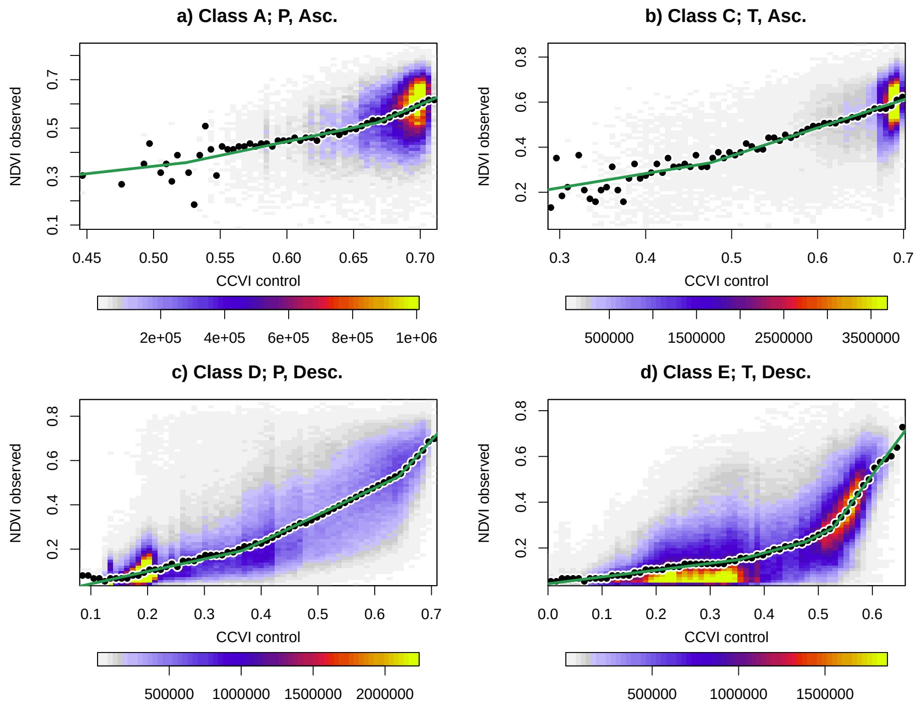

Figure 3. Bias adjustment of the CCVI. Dots indicate median observed NDVI per interval of CCVI (the CCVI was divided in 64 equidistant intervals). The green line shows the function obtained with segmented regression through the median points. **(a)** Relationship between modelled CCVI and observed NDVI for KT Region A for precipitation constraints and ascending NDVI. **(b)** Same as **(a)** but for class B and temperature constraints. **(c)** Same as a but for KT class D and descending NDVI. **(d)** Same as **(b)** but for KT class E.

GMDD
8, 4781–4821, 2015

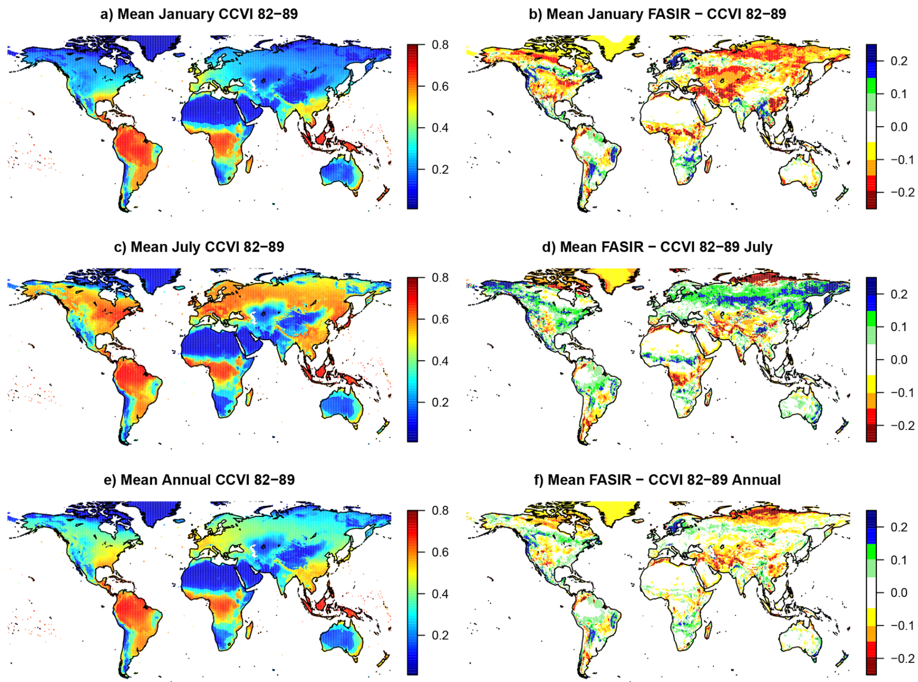

Figure 4. (a) Mean January CCVI 1982–1989. **(b)** Difference between observations and **(a)**. **(c)** Mean July CCVI 1982–1989. **(d)** Difference between observations and **(c)**. **(e)** Mean annual CCVI 1982–1989. **(f)** Difference between observations and **(e)**.

GMDD
8, 4781–4821, 2015

Title Page
Abstract | Introduction
Conclusions | References
Tables | Figures
Back | Close
Full Screen / Esc
Printer-friendly Version
Interactive Discussion

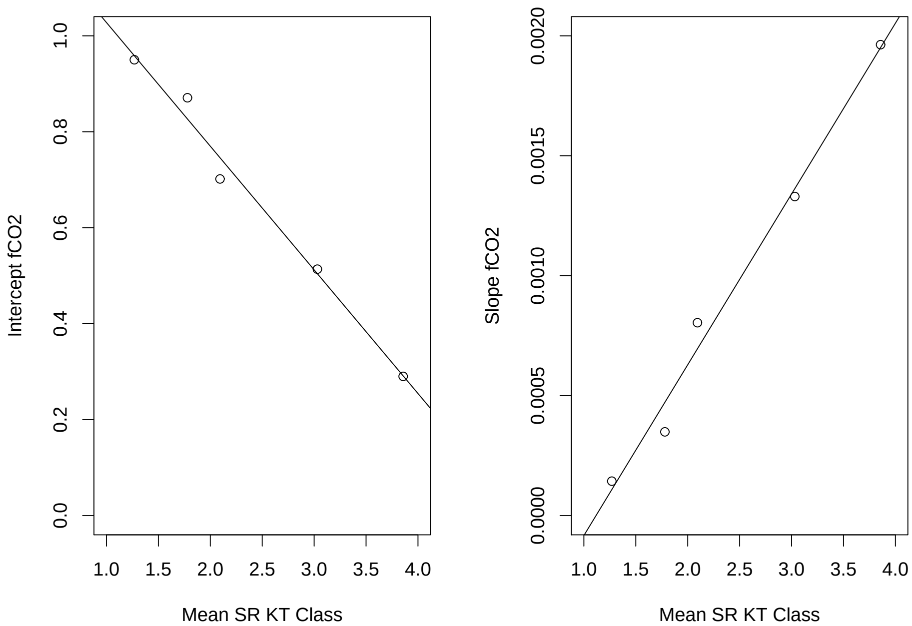

Figure 5. Change in CO_2 fertilisation effect as a function of mean SR per KT climate zone; the intercept and slope vary linearly with simple ratio (SR) (see Eqs. 1 and 2).

GMDD
8, 4781–4821, 2015

Climate related variability in vegetation greenness

S. O. Los

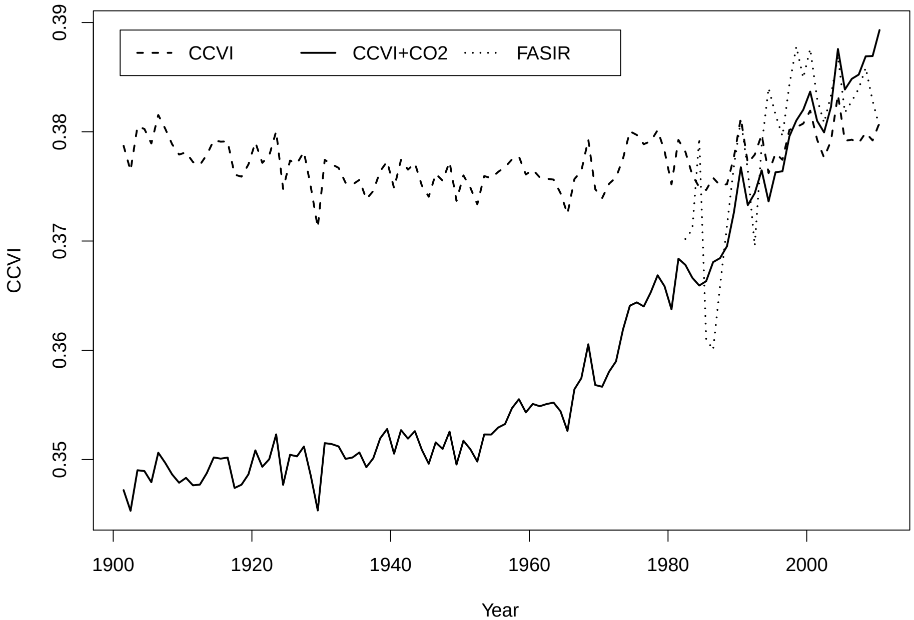

Figure 6. Time series of mean global annual CCVI with and without CO_2 fertilisation from 1901–2010. FASIR NDVI is shown from 1982–2010.

GMDD
8, 4781–4821, 2015

Climate related variability in vegetation greenness

S. O. Los

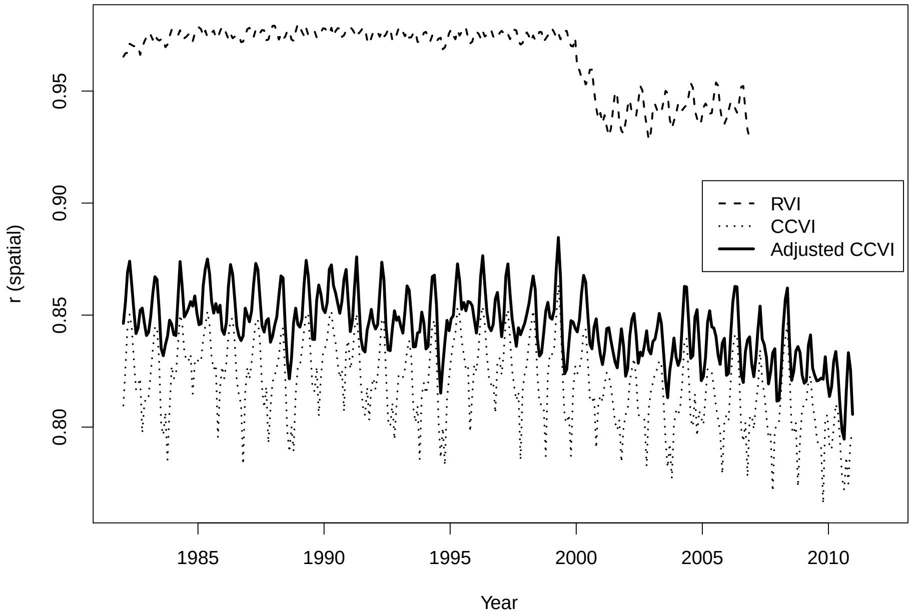

Figure 7. Time series of monthly spatial correlation between $CCVI_{Cad}$ and FASIR NDVI (solid line). Shown for comparison are the spatial correlations for RVI (dashed line) and $CCVI_{control}$ (dotted line). RVI has the highest spatial correlations with FASIR NDVI but shows a decrease from about $r = 0.97$ to about $r = 0.93$ after 2000. A smaller downward deviation from about $r = 0.84$ to about $r = 0.82$ occurs in the CCVI correlations. The average monthly spatial correlation for latitudes above 30° N (not shown) is $r = 0.75$.

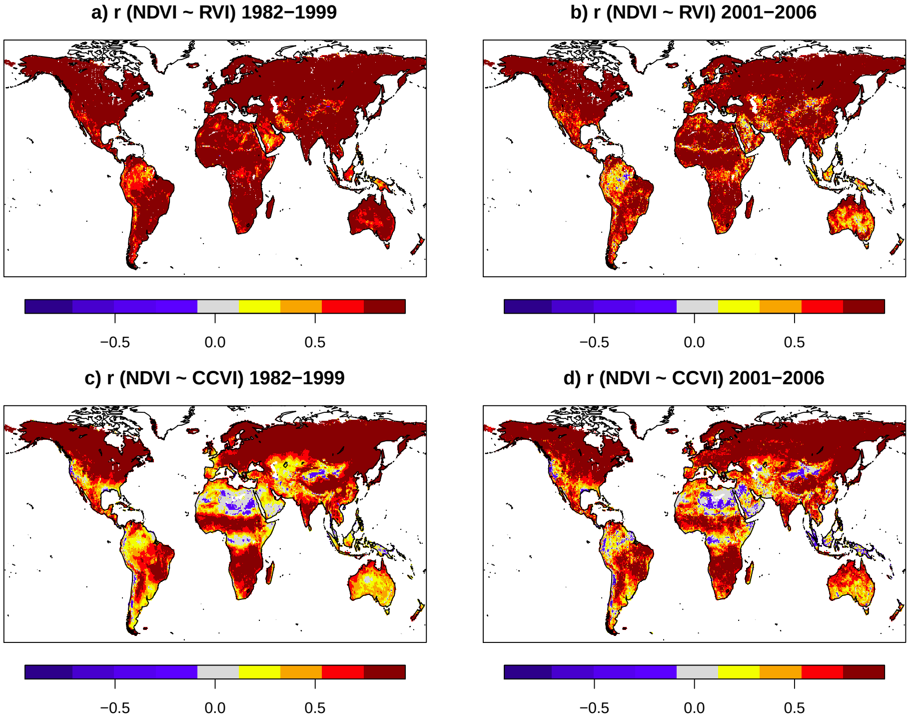

Figure 8. (a) Spatial distribution of temporal correlations between RVI (Los, 2013) and FASIR NDVI for 1982–1999 (training period). **(b)** Same as **(a)** but for 2001–2006. **(c)** Temporal correlations between CCVI and FASIR NDVI for 1982–1999; **(d)** same as **(c)** but for 2001–2006.

GMDD
8, 4781–4821, 2015

Climate related variability in vegetation greenness

S. O. Los

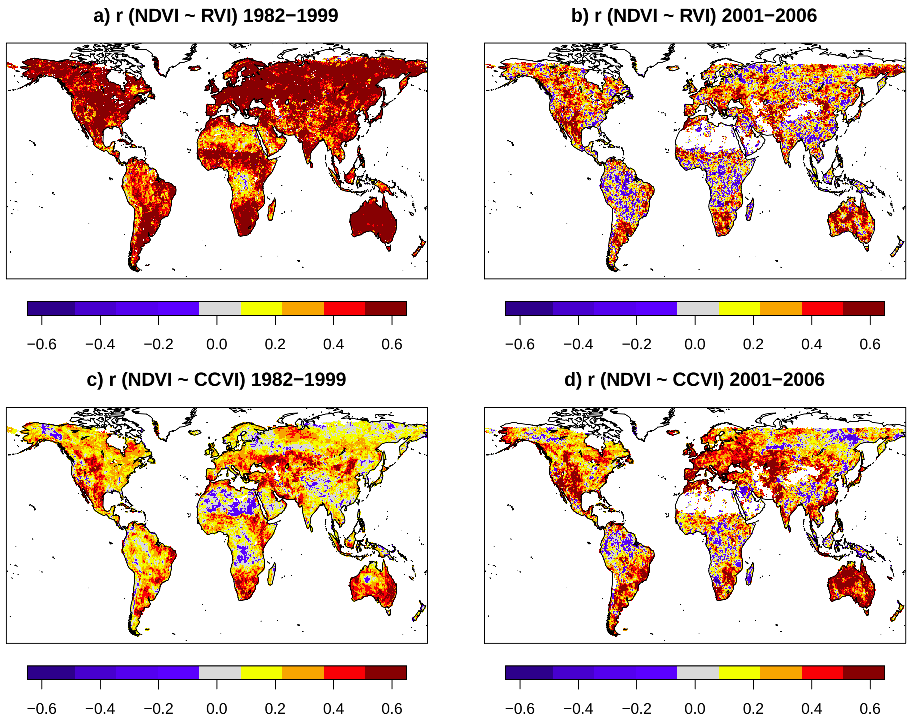

Figure 9. (a) Spatial distribution of temporal correlations between RVI and FASIR NDVI anomalies for 1982–1999 (training period). **(b)** Same as **(a)** but for 2001–2006 (outside training period; mean $r = 0.188$. **(c)** Temporal correlations between CCVI and FASIR NDVI anomalies for 1982–1999. **(d)** Same as **(c)** but for 2001–2006, mean $r = 0.255$ – significantly higher at $p < 2.210^{-16}$ than $r = 0.188$ for the RVI under **(b)**.

Discussion Paper | Discussion Paper | Discussion Paper | Discussion Paper |
GMDD
8, 4781–4821, 2015

Climate related variability in vegetation greenness

S. O. Los

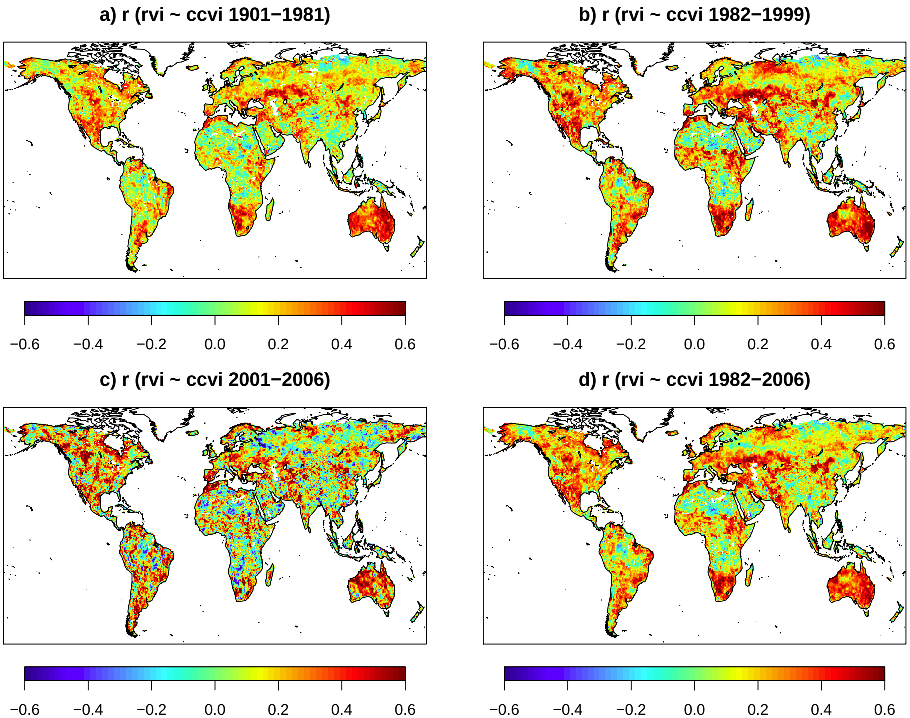

Figure 10. Temporal correlations between RVI (control) and CCVI (control) monthly anomalies for **(a)** 1901–1981, **(b)** 1982–1999, **(c)** 2001–2006, and **(d)** 1982–2006.

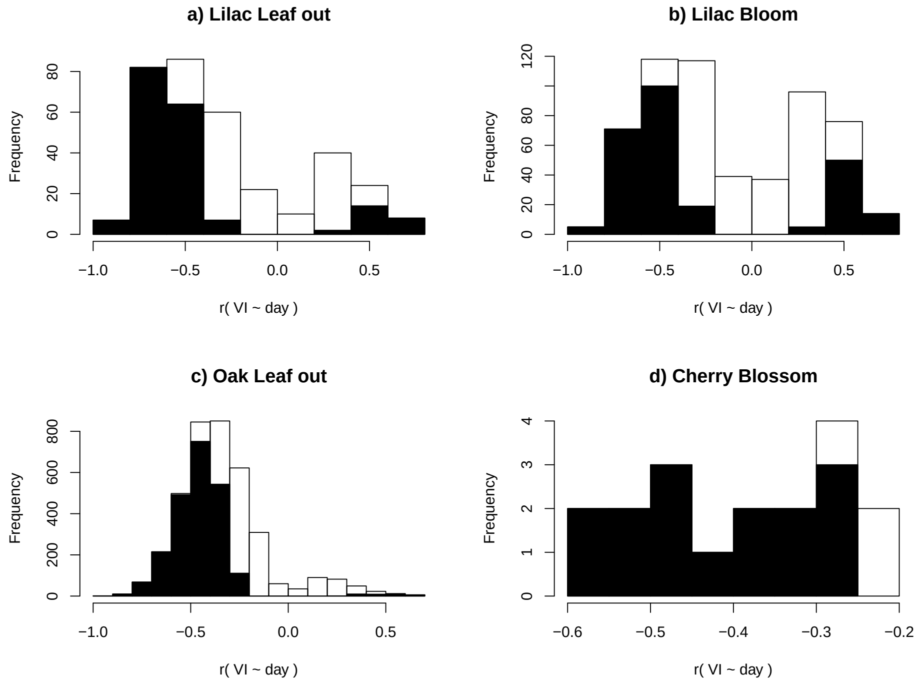

Figure 11. Frequency distributions of maximum correlations between day of leaf out (or first day of bloom) and CCVI of previous, concurrent or next month. Black indicates correlations significant at $p < 0.1$; white bars show correlations that are not significant. **(a)** Correlations for day of lilac leaf out. **(b)** For day of lilac blossom. **(c)** For German oak leaf out. **(d)** Cherry blossom in former Soviet Union. CCVI correlations were significantly more negative (larger absolute value) than RVI correlations for German oak (mean $r = -0.34$ vs. mean $r = -0.29$ respectively with $p \ll 0.01$) and for cherry blossom ($r = -0.38$ vs. $r = -0.22$; $P < 0.01$). RVI and CCVI correlations with cherry blossom were not significantly different. Correlation of CCVI with Marsham Oak data for 1901–1958 (Sparks and Carey, 1995) is −0.41 compared to −0.78 for the RVI data (Los, 2013).

GMDD
8, 4781–4821, 2015

Climate related variability in vegetation greenness

S. O. Los

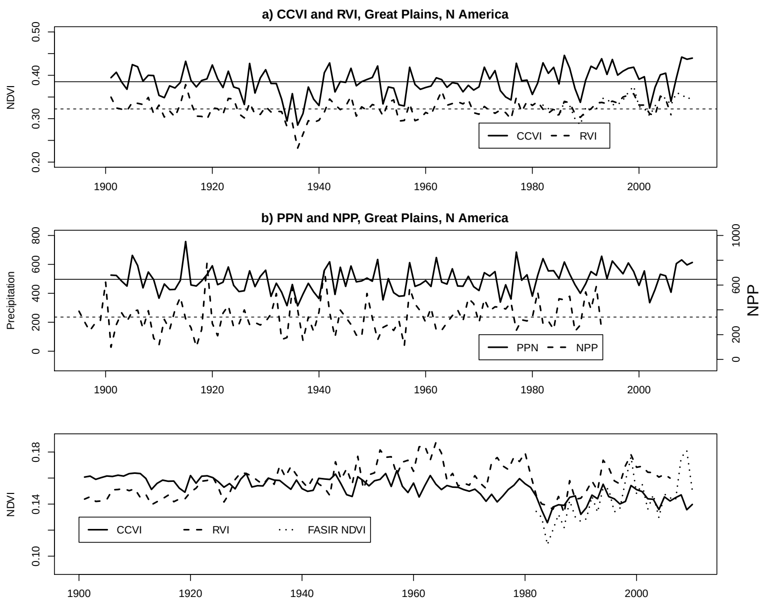

Figure 12. Impact of extreme drought on the CCVI. **(a)** CCVI and RVI time series for the northern US Plains between 40.5–45.5° N and 99–101.5° W, both showing severely depressed vegetation during the 1930s dust bowl; the CCVI also shows negative excursions during the 1950s. **(b)** As **(a)** but for CRU precipitation and CENTURY NPP (Metherall et al., 1993). Precipitation shows negative anomalies similar to the CCVI whereas the CENTURY NPP does not show negative anomalies. Coefficient of correlations between precipitation (1901–1993) and CCVI: $r = 0.83$; RVI $r = 0.60$ and CENTURY NPP $r = 0.17$. **(c)** CCVI and RVI time series for the Sahel in Sudan between 12.5–15° N and 23–34° E with FASIR NDVI data added for comparison. Both CCVI and RVI indicate a drought in 1984. Correlations for precipitation 1901–2006 with CCVI $r = 0.71$; and with RVI $r = 0.80$; for 1982–2006: correlation of precipitation with CCVI $r = 0.64$; with RVI $r = 0.70$ and with FASIR NDVI $r = 0.74$. Correlation between FASIR NDVI and RVI ($r = 0.89$) and between FASIR NDVI and CCVI ($r = 0.80$).

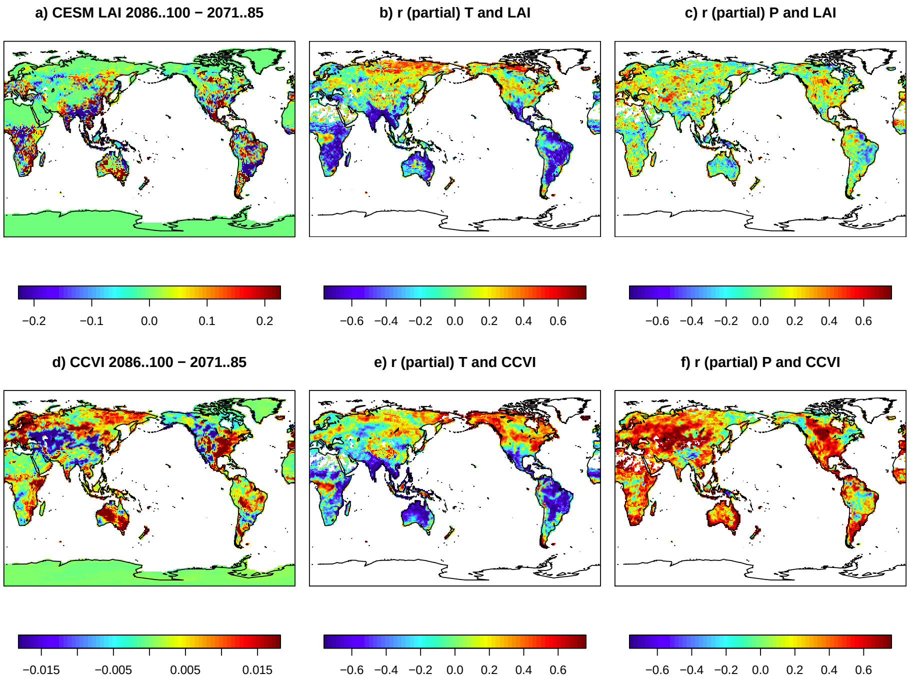

Figure 13. Comparison of the response of CCVI and CESM LAI to changes in CESM precipitation and temperature between 2071–2100. **(a)** Difference mean LAI 2086–2100 and mean LAI 2071–2085. **(b)** Partial correlations between mean annual temperature and mean annual LAI for 2071–2100. **(c)** Partial correlations between annual precipitation and mean annual LAI for 2071–2100. **(d–f)** Same as **(a–c)** but for CCVI. Both CCVI and LAI have negative correlations with temperature in (semi-arid) tropical regions. Partial correlations between CCVI and precipitation are higher than partial correlations between LAI and precipitation in mid-to-high northern latitude. The MPI and HadGEM analyses are provided in the Supplement.

GMDD
8, 4781–4821, 2015